Effects of Li and Cu dopants on structural properties of zinc oxide nanorods

Kyung Ho Kim*, Zhuguang Jin, Yoshio Abe, Midori Kawamura

Department of Materials Science and Engineering, Kitami Institute of Technology, 165 Koen-cho, Kitami, Hokkaido 090-8507, Japan

Abstract

We fabricated undoped zinc oxide (ZnO), Li-doped zinc oxide (LZO), and Cu-doped zinc oxide (CZO) nanorods (NRs) on fluorine-doped tin oxide (FTO)-coated glass substrates using chemical solution deposition and investigated their structural properties. With the incorporation of the Li dopant, the length and crystallinity of LZO NRs increased and improved, respectively, compared to that of the ZnO NRs. The average optical transmittance of LZO NRs was slightly lower than that of the ZnO NRs, but otherwise very similar over the visible wavelength region. With the incorporation of the Cu dopant, however, the morphology of the CZO sample was remarkably different from that of the pure ZnO NRs. Rods with a length of ~12 μm and a diameter of 0.5-1.2 μm

were randomly oriented on the substrate, and copper oxide (CuO) nanocrystals were uniformly grown on the surface of substrate. This paper presents a simple way to tune the growth behaviors of the ZnO NRs by adding dopants.

Keywords: ZnO; Li; Cu; Dopant; Nanorods; Morphology

Corresponding author: Kyung Ho Kim, Tel: 81-157-26-9431, Fax: 81-157-26-4973,

E-mail address: khkim@mail.kitami-it.ac.jp

1. Introduction

The wide-bandgap semiconductor zinc oxide (ZnO) has a large exciton binding energy (60 meV) at room temperature, nontoxicity, chemical and photochemical stability, and raw materials abundance [1-3]. Because of these properties, ZnO has attracted considerable attention in a wide range of applications such as polariton lasers, light-emitting diodes (LEDs), photovoltaic (PV) cells, thin film transistors (TFTs), piezoelectrics, and chemical sensors [1-6]. In particular, one-dimensional (1D) ZnO nanostructures are among the most important materials for applications in nanoscale electronic and optoelectronic devices [4-10].

The methods used for fabricating ZnO NRs include solution methods, thermal evaporation, sputtering, molecular beam epitaxy (MBE), metal-organic chemical vapor deposition (MOCVD), and pulsed laser deposition (PLD). Solution methods have many advantages, including low-cost manufacturing, simplicity, easy control of compositions, and great potential for scale-up [11-15].

In our previous study, we reported the structural properties of ZnO NRs grown on a ZnO seed layer using solution methods with various seed annealing temperatures [16]. Long and well-aligned ZnO NRs were obtained at seed annealing temperature of 350 ºC because the seed layer has a larger particle size and high crystallinity at this

temperature.

On the other hand, a widely used strategy for tuning the physical properties of ZnO is to use metallic dopants (Cu, Ni, Ag, Al, etc.) [17-19]. In this study, we grew Li-doped ZnO (LZO) and Cu-doped ZnO (CZO) NRs on ZnO seed layers that were prepared on fluorine-doped tin oxide (FTO)-coated glass substrates. The structural and optical properties of Li- and Cu-doped ZnO NRs and undoped ZnO NRs were characterized by X-ray diffraction (XRD), field emission scanning electron microscopy (FESEM), and ultraviolet-visible (UV-Vis) spectroscopy.

2. Experimental

2.1 Preparation of ZnO seed layers

ZnO seed layers were prepared by sol-gel spin-coating. A zinc acetate dihydrate ($Zn(CH_3COO)_2 \cdot 2H_2O$, 0.25 M, Wako) precursor was dissolved in ethanol (C_2H_6O, Wako), 2-methoxyethanol (ME) ($C_3H_8O_2$, Wako), and Milli-Q. After being stirred for 1 h at 60 ºC, the sol was aged at room temperature for 24 h. The FTO-coated glass substrates were prepared by cleaning in an ultrasonic bath with acetone and isopropyl alcohol for 10 min each, followed by exposure to UV-ozone (Filgen, UV 253FS) for 45 min. The sol was spin-coated onto the prepared substrates at 2000 rpm for 30 s and

dried at 250 ºC for 5 min. Subsequently, it was annealed at 350 ºC for 30 min in a furnace at heating rate of 10 ºC/min. The thickness of the seed layer, measured by variable-angle ellipsometry (MIZOJIRI, DVA-FL), was ~35 nm.

2.2 Preparation of ZnO, LZO, and CZO NRs

ZnO, Li-doped ZnO (LZO), and Cu-doped ZnO (CZO) NRs were grown by chemical solution deposition on the ZnO seed layers. An aqueous solution of zinc nitrate hexahydrate ($Zn(NO_3)_2 \cdot 6H_2O$, 0.01 M, Sigma-Aldrich) and hexamethylenetetramine (HMT) ($C_6H_{12}N_4$, 0.01 M, Sigma-Aldrich) was prepared. Lithium chloride hydrate ($LiCl \cdot xH_2O$, 5 mM, Sigma-Aldirch) and copper acetate monohydrate ($Cu(CO_2CH_3)_2 \cdot H_2O$, 5 mM, Wako), which provide the Li and Cu dopants, respectively, were added to the solution. The solution was stirred for 1 h at room temperature. The ZnO seed layers were then vertically dipped and held there at 90 ºC for 6 h. Next, the samples were rinsed in deionized water several times and finally dried at 120 ºC for 10 min in air.

2.3 Characterization methods

The surface morphology of the seed layer was examined by atomic force

microscopy (AFM) (SHIMADZU, SPM-9500J3). The crystal structure and orientation of the NRs were characterized by XRD (Bruker, D8 ADVANCE) with a CuKα radiation source. The morphology and chemical composition of the NRs were examined by FESEM (JEOL, JSM-6701F) combined with energy dispersive X-ray spectroscopy (EDS). Optical transmission properties were studied by UV-Vis spectroscopy (HITACHI, U-2910) with a wavelength range of 200-800 nm.

3. Results and discussion

Figure 1(a) shows an AFM image of the bare FTO-coated glass substrate. It shows that the FTO is composed of nanoparticles 100 nm in diameter. The root mean square (RMS) roughness of the FTO is ~20.3 nm. The AFM image of the ZnO seed layer prepared on the FTO-coated glass substrate is shown in Fig. 1(b). The RMS roughness of the ZnO is ~16.2 nm. This means that the seed layer effectively smoothed the rough surface of the bare substrate. The average size of the seed nanoparticles is 20 nm.

Figure 2(a) shows the top view FESEM image of the ZnO NRs. The inset image in Fig. 2(a) shows a cross-section. The NRs are uniformly grown on the surface of the seed layer and aligned perpendicular to the FTO-coated glass substrate. The average length, diameter, and surface density of the NRs are 1.2 μm, 35 nm, and 168 μm^{-2}, respectively.

The FESEM images (top view and inset cross-sectional view) of LZO NRs are shown in Fig. 2(b). With the incorporation of the Li dopant, the average length and diameter are 1.7 μm and 35 nm, respectively, whereas, the surface density decreased to 135 μm^{-2}. As the LZO NRs increase in length, they display the phenomenon of self-attraction, as seen in the top view FESEM image (Fig. 2(b)) [20,21]. The growth rate of the NRs is clearly dependent on the Li dopant, which led to distinct aspect ratios (34 for ZnO NRs and 48 for LZO NRs). Aside from this change in aspect ratio with Li doping, no other morphological change was observed.

Figure 3 shows the XRD patterns of ZnO NRs and LZO NRs. It is clear that all diffraction peaks belong to the hexagonal wurtzite ZnO phase (JCPDS card no. 36-1451). No other impurity peaks are observed within the precision limit of the XRD measurement, indicating no secondary phase in the samples. All NRs show the strongest diffraction peak corresponding to the (002) plane. It is well known that the *c*-axis is the preferred orientation of ZnO because of the low surface free energy of the (002) plane [22,23]. The diffraction angle 2θ of (002) is 34.44º for ZnO NRs and 34.42 º for LZO NRs. This difference is consistent with the fact that the ionic radius of Li^+ (0.76 Å) is slightly larger than that of Zn^{2+} (0.74 Å) [24,25]. This difference in ionic radius resulted in a lower diffraction angle, corresponding to an increased *c*-lattice parameter of LZO

NRs (5.206 Å) than of ZnO NRs (5.204 Å). It should be noted that the intensity of (002) peak increases with incorporation of Li dopant. This may because the Li atoms easily substituted Zn atoms in the lattice, and yielded better crystallinity and *c*-axis orientation [18]. Vertically well-aligned NRs plays a vital role in the fabrication of nanoscale electronics and optoelectronics. The XRD results are in agreement with the FESEM results (Fig. 3 and Fig. 2, respectively).

Figure 4(a) shows the optical transmittance spectra of the ZnO NRs and LZO NRs. The ZnO NRs show high transmittance (~80%) of visible wavelengths. The transmittance of LZO NRs is lower than that of the ZnO NRs, but otherwise very similar [25]. As shown in Fig. 4(b), the optical bandgaps, estimated from the plots of $(\alpha h\nu)^2$ versus photon energy $h\nu$, of ZnO NRs and LZO NRs are 3.29 and 3.30 eV, respectively [25]. Optical transmission property of NRs in the visible wavelengths is strongly important factor affecting the performance of photovoltaic cells. With incorporation of the Li dopant, long and well-aligned NZO NRs exhibit good optical transparency.

Figure 5(a) shows the top view FESEM image of the CZO sample. The inset image in Fig. 5(a) is a cross-sectional FESEM image. It is noteworthy that the surface morphology of the CZO sample is significantly different from the ZnO NRs and LZO

NRs. The CZO rods are hexagonal and very large, with a remarkable length of ~12 μm. The diameter ranges from 0.5 to 1.2 μm, and the rods are slightly narrower at the top than at the bottom. Most of the rods are randomly inclined on the substrate. It should be noted that NRs, with diameters on the order of tens of nanometers, are not observed anywhere on the surface of substrate. Figure 5(b) shows the high magnification image of the dashed rectangular region marked in Fig. 5(a). Interestingly, this sample also contains rice-shaped nanoparticles with a length of ~300 nm and a width of ~100 nm, which are uniformly distributed on the surface of the substrate. The mean thickness of this layer of nanoparticles, estimated from inset image in Fig. 5(b), is 300 nm.

Table 1 presents the results of EDS analysis of the composition (in atomic percent) of the ZnO and CZO samples. Compared to the ZnO NRs, the CZO rods were slightly oxygen deficient and zinc rich. The Zn and Cu atomic percentages of the CZO sample in the rod region (A in Fig. 5(a)) and in the nanoparticle region (B in Fig. 5(b)) are 41.1% and 2.4%, and 8.6% and 21.6%, respectively. The EDS analysis shows that the nanoparticle region is Cu-rich and Zn-deficient.

Figure 6 shows the XRD pattern of the CZO sample. The major diffraction peaks correspond to the (100), (002), (101), (102), and (110) planes of hexagonal wurtzite ZnO (JCPDS card no. 36-1451). The two weak peaks at 35.51º and 38.72º correspond to

the (002) and (111) planes of monoclinic CuO (JCPDS card no. 01-080-1917). The EDS and XRD results suggest that a secondary phase of CuO nanoparticles was formed on the surface of the substrate when the amount of Cu dopant exceeded the solubility limit in the ZnO (~10%) [26,27]. The optical transmittance of the CZO sample (not shown) is quite low (< 20%) due to the presence of CuO, which strongly absorbs throughout the visible spectrum [28].

4. Conclusions

We investigated the structural properties of ZnO, LZO, and CZO NRs grown on ZnO seed layers on FTO-coated glass substrates. The Li and Cu dopants had remarkably different influences on the growth behavior of the ZnO NRs. Incorporating the Li dopant in the solution provided a facile way to produce long and well-aligned NRs with high crystallinity. ~~The optical transmittance of the LZO NRs was slightly lower than that of ZnO NRs over the visible wavelength region, but otherwise very similar.~~ By contrast, the addition of the Cu dopant induced significant morphological changes in the NRs. Instead of the vertically aligned NRs with diameters on the order of several nanometers, large and randomly-oriented rods with lengths of ~12 μm and diameters in the range of 0.5-1.2 μm were grown on the surface of the FTO-coated glass substrate.

~~The Cu dopant that exceeded the solubility limit in the ZnO formed CuO nanocrystals on the surface of the substrate.~~ Our results indicate that by choosing dopants, it could be possible to easily control the growth behaviors of ZnO NRs.

Acknowledgement

This work was supported by the Grant-in-Aid for Young Scientists (B) (24760245) from the Japan Society for the Promotion of Science (JSPS).

Figure captions

Fig. 1. AFM images of (a) bare FTO-coated glass substrate and (b) ZnO seed layer prepared on FTO-coated glass substrate.

Fig. 2. Top view FESEM images of (a) ZnO NRs and (b) LZO NRs. Inset images are cross-sectional images.

Fig. 3. XRD patterns of ZnO NRs and LZO NRs on the FTO-coated glass substrates.

Fig. 4. (a) UV-Vis transmittance spectra and (b) plots of $(\alpha h\nu)^2$ versus $h\nu$ of the ZnO NRs and LZO NRs on the FTO-coated glass substrates.

Fig. 5. Top-view FESEM images of CZO sample; (a) low and (b) high magnification images. Inset images in (a,b) are cross-sectional images. The dotted lines in (a) indicate the areas that are presented in higher magnification in (b).

Fig. 6. XRD pattern of CZO sample on the FTO-coated glass substrate.

Table 1. Atomic percentage of compositional elements of ZnO NRs and CZO samples, obtained from EDS analysis.

Samples		Atomic percentage of element (%)		
		O	Zn	Cu
ZnO NRs		61.2	38.8	-
CZO	rods	56.5	41.1	2.4
	nanoparticles	69.8	8.6	21.6

References

[1] S.J. Pearton, D.P. Norton, K. Ip, Y.W. Heo, T. Steiner, Recent progress in processing and properties of ZnO, Prog. Mater. Sci. 50 (2005) 293-340.

[2] E. Fortunato, A. Gonçalves, A. Pimentel, P. Barquinha, G. Gonçalves, L. Pereira, I. Ferreira, R. Martins, Zinc oxide, a multifunctional material: from material to device applications, Appl. Phys. A 96 (2009) 197-205.

[3] M. Zamfirescu, A. Kavolin, B. Gil, G. Malpuech, M. Kaliteevski, ZnO as a material mostly adapted for the realization of room-temperature polariton lasers, Phys. Rev. B 65 (2002) 161205.

[4] X.B. Wang, C. Song, D.M. Li, K.W. Geng, F. Zeng, F. Pan, The influence of different doping elements on microstructure, piezoelectric coefficient and resistivity of sputtered ZnO film, Appl. Surf. Sci. 253 (2006) 1639-1643.

[5] F. Xu, L. Sun, Solution-derived ZnO nanostructures for photoanodes of dye-sensitized solar cells, Energy Environ. Sci. 4 (2011) 818-841.

[6] Y. Zhang, M.K. Ram, E.K. Stefanakos, D.Y. Goswami, Synthesis, characterization, and applications of ZnO nanowires, J. Nanomater. 2012 (2012) Article ID 624520.

[7] Z.L. Wang, J. Song, Piezoelectric nanogenerators based on zinc oxide nanowire arrays, Science 312 (2006) 242-246.

[8] J.G. Lu, P. Chang, Z. Fan, Quasi-one-dimensional metal oxide materials-Synthesis, properties and applications, Mater. Sci. Eng. R 52 (2006) 49-91.

[9] P. Yang, H. Yan, S. Mao, R. Russo, J. Johnson, R. Saykally, N. Morris, J. Pham, R. He, H-J. Choi, Controlled growth of ZnO nanowires and their optical properties, Adv. Funct. Mater. 12 (2002) 323-331.

[10] A. Pimentel, D. Nunes, P. Duarte, J. Rodrigues, F.M. Costa, T. Monteiro, R. Martins, E. Fortunato, Synthesis of long ZnO nanorods under microwave irradiation or conventional heating, J. Phys. Chem. C 118 (2014) 14629-14639.

[11] Y.W. Heo, K. Ip, S.J. Pearton, D.P. Norton, J.D. Budai, Growth of ZnO thin films on *c*-plane Al_2O_3 by molecular beam epitaxy using ozone as an oxygen source, Appl. Surf. Sci. 252 (2006) 7442-7448.

[12] K.A. Wahid, W.Y. Lee, H.W. Lee, A.S. The, D.C.S. Bien, I.A. Azid, Effect of seed annealing temperature and growth duration on hydrothermal ZnO nanorod structures and their electrical characteristics, Appl. Surf. Sci. 283 (2013) 629-635.

[13] K. Song, D. Kim, X-S. Li, T. Jin, Y. Jeong, J. Moon, Solution processed invisible all-oxide thin film transistors, J. Mater. Chem. 19 (2009) 8881-8886.

[14] B.S. Ong, C. Li, Y. Li, Y. Wu, R. Loutfy, Stable, solution-processed, high-mobility ZnO thin-film transistors, J. Am. Chem. Soc. 129 (2007) 2750-2751.

[15] M-J. Jin, S-D. Lee, K-S. Shin, S-W. Jeong, D.H. Yoon, D. Jeon, I-H. Lee, D.K. Lee, S-W. Kim, Low-temperature solution-based growth of ZnO nanorods and thin films on Si substrates, J. Nanosci. Nanotechnol. 9 (2009) 1-4.

[16] K.H. Kim, K. Utashiro, Y. Abe, M. Kawamura, Growth of zinc oxide nanorods using various seed layer annealing temperatures and substrate materials, Int. J. Electrochem. Sci. 9 (2014) 2080-2089.

[17] M. Bakikier, D. Wang, J. Wang, Q. Li, J. Sun, Y. Yan, Q. Yu, S. Jiao, Cu-doped ZnO nanorod arrays: the effects of copper precursor and concentration, Nanoscale Res. Lett. 9 (2014) 199-1-9.

[18] A. Yavuz Oral, Z. Banu Bahşi, M. Hasan Aslan, Microstructure and optical properties of nanocrystalline ZnO and ZnO:(Li or Al) thin films, Appl. Surf. Sci. 253 (2007) 4593-4598.

[19] Y. Chen, X.L. Xu, G.H. Zhang, H. Xue, S.Y. Ma, A comparative study of the microstructures and optical properties of Cu- and Ag-doped ZnO thin films, Phys. B 404 (2009) 3645-3649.

[20] X. Han, G. Wang, L. Zhou, J.G. Hou, Crystal orientation-ordered ZnO nanorod bundles on hexagonal heads of ZnO microcones: epitaxial growth and self-attraction, Chem. Commun. 8 (2006) 212-214.

[21] S. Lin, H. Hu, W. Zheng, Y. Qu, F. Lai, Growth and optical properties of ZnO nanorod arrays on Al-doped ZnO transparent conductive film, Nanoscale Res. Lett. 8 (2013) 158-1-6.

[22] N. Fujimura, T. Nisihhara, S. Goto, J. Xu, T. Ito, Control of preferred orientation of ZnO_x films: control of self-texture, J. Cryst. Growth 130 (1993) 269-279.

[23] L. Xu, X. Li, Y. Chen, F. Xu, Structural and optical properties of ZnO thin films prepared by sol-gel method with different thickness, Appl. Surf. Sci. 257 (2011) 4031-4037.

[24] R.D. Shannon, Revised effective ionic radii and systematic studies of interatomic distances in halides and chalcogenides, Acta Cryst. A 32 (1976) 751-767.

[25] M. Caglar, Y. Caglar, S. Aksoy, S. Ilican, Temperature dependence of the optical band gap and electrical conductivity of sol-gel derived undoped and Li-doped ZnO films, Appl. Phys. Lett. 256 (2010) 4966-4971.

[26] S. Singhal, J. Kaur, T. Namgyal, R. Sharma, Cu-doped ZnO nanoparticles: Synthesis, structural and electrical properties, Physica B 407 (2012) 1223-1226.

[27] M. Mukhtar, L. Munisa, R. Saleh, Co-precipitation synthesis and characterization of nanocrystalline zinc oxide particles doped with Cu^{2+} ions, Mater. Sci. Appl. 3 (2012) 543-551.

[28] F. Marabelli, G.B. Parravicini, F. Salghetti-Drioli, Optical gap of CuO, Phys. Rev. B 52 (1995) 1433-1436.

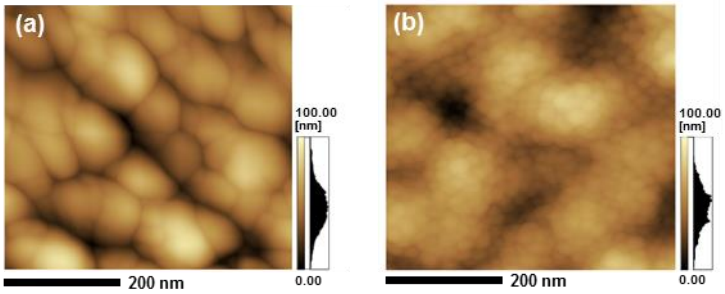

Fig. 1.

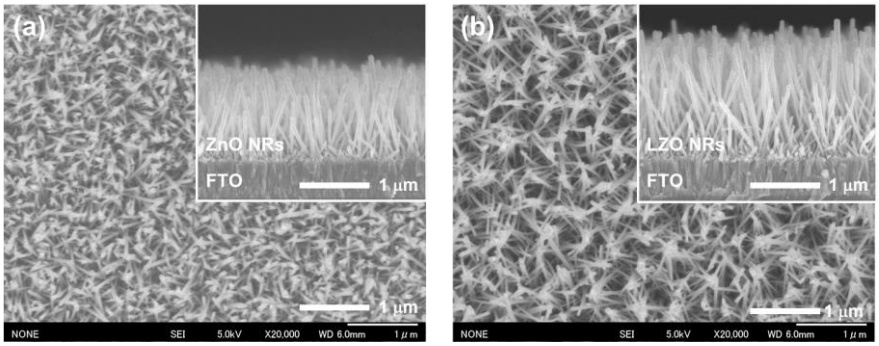
(a)
ZnO NRs
FTO
1 μm
1 μm
NONE SEI 5.0kV X20,000 WD 6.0mm 1 μm
(b)
LZO NRs
FTO
1 μm
1 μm
NONE SEI 5.0kV X20,000 WD 6.0mm 1 μm

Fig. 2.

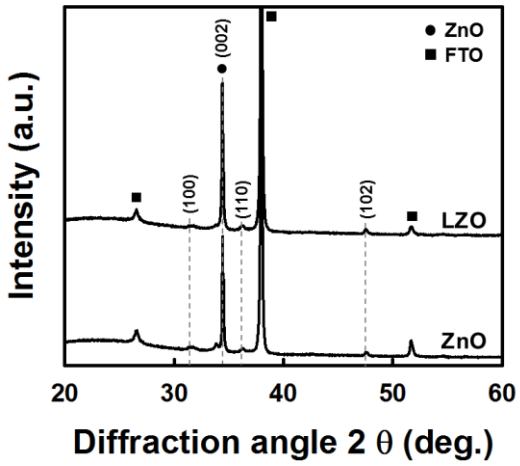
● ZnO
■ FTO
(002)
(100)
(110)
(102)
LZO
ZnO
Intensity (a.u.)
20
30
40
50
60
Diffraction angle 2 θ (deg.)

Fig. 3.

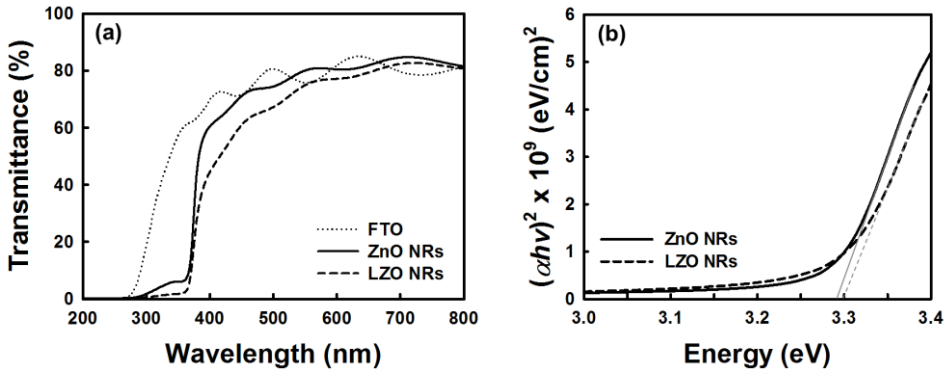
(a)
Transmittance (%)
Wavelength (nm)
FTO
ZnO NRs
LZO NRs
(b)
$(\alpha hv)^2$ x 10^9 (eV/cm)^2
Energy (eV)
ZnO NRs
LZO NRs

Fig. 4.

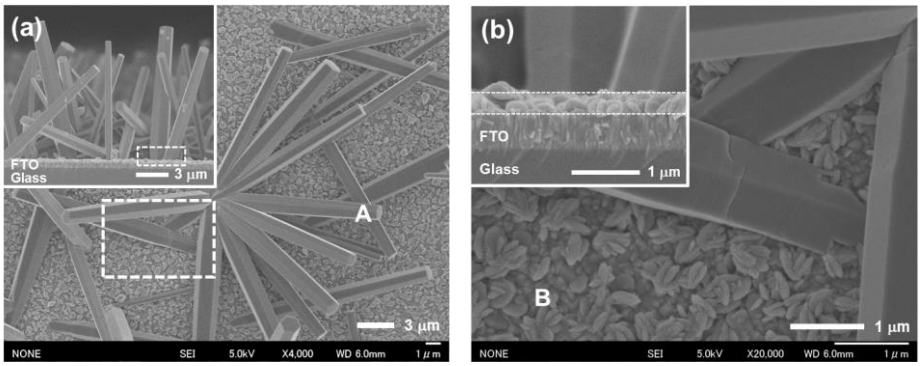
(a)
FTO
Glass
3 μm
A
3 μm
NONE SEI 5.0kV X4,000 WD 6.0mm 1 μm
(b)
FTO
Glass
1 μm
B
1 μm
NONE SEI 5.0kV X20,000 WD 6.0mm 1 μm

Fig. 5.

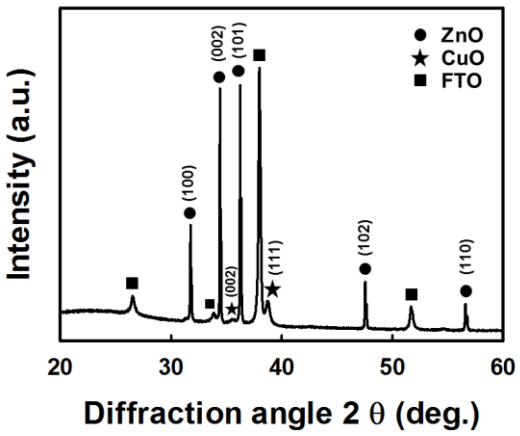
ZnO
CuO
FTO
(002)
(101)
(100)
(002)
(111)
(102)
(110)
Intensity (a.u.)
20
30
40
50
60
Diffraction angle 2 θ (deg.)

Fig. 6.